

Synthesis and characterization of FeNi₃@SiO₂@TiO₂ nano-composite and its application as a catalyst in a photochemical oxidation process to decompose tetracycline

Maryam Khodadadi^a, Susana Rodriguez-Couto^b, Fatemeh Sadat Arghavan^c,
Ayat Hossein Panahi^{d,*}

^aMedical Toxicology and Drug abuse Research Center (MTDRC), Birjand University of Medical Sciences (BUMS), Birjand, Iran, email: maryam.khodadadi@gmail.com (M. Khodadadi)

^bIkerbasque, Basque Foundation for Science, Maria Diaz de Haro 3, 48013 Bilbao, Spain, email: susanarodriguezcouto@gmail.com (S. Rodriguez-Couto)

^cStudent Research Committee, Social Determinants of Health Research Center, Faculty of Health, Mashhad University of Medical Sciences, Mashhad, Iran, email: fatemeh.arghavan71@gmail.com (F.S. Arghavan)

^dSocial Determinants of Health Research Center, Birjand University of Medical Sciences, Birjand, Iran, email: ayatpanahi@yahoo.com (A. Hossein Panahi)

Received 26 September 2019; Accepted 20 March 2020

ABSTRACT

The aim of the present study was the synthesis of the FeNi₃@SiO₂@TiO₂ nanocomposite and its application as a catalyst to degrade the antibiotic tetracycline (TC) from aqueous solutions. For this, first, FeNi₃@SiO₂@TiO₂ nanocomposite was synthesized by a sol-gel method and then it was characterized by means of different techniques. Thus, according to X-ray diffraction, Fourier transformed infrared spectroscopy, and field-emission scanning electron microscopy the mean crystal size of the FeNi₃@SiO₂@TiO₂ nanocomposites was 77 nm and had a high tendency to form agglomerates. Also, the analysis of VSM showed that the nanocomposites had magnetic properties. In addition, the thermal gravimetric analysis technique showed that the FeNi₃@SiO₂@TiO₂ nanoparticles presented a high resistance to heat. Further, the synthesized nanocomposite was applied for the degradation of TC from aqueous solutions in a UV/H₂O₂/FeNi₃@SiO₂@TiO₂ process. Complete degradation of TC was achieved operating under optimal conditions (i.e., pH = 5, FeNi₃@SiO₂@TiO₂ dose = 0.01 g/L, TC initial concentration = 20 mg/L, H₂O₂ concentration = 150 mg/L and reaction time = 90 min). Therefore, the UV/H₂O₂/FeNi₃@SiO₂@TiO₂ process holds great potential for pharmaceuticals degradation.

Keywords: FeNi₃@SiO₂@TiO₂ magnetic nanocomposite; UV/H₂O₂/FeNi₃@SiO₂@TiO₂ reactions; Degradation; Tetracycline; Kinetics

1. Introduction

In the last decade, drug combinations have been considered as one of the most important water contaminants due to their high diversity and massive utilization [1–3]. The consumption of drugs in high amounts has caused

the entry of the remaining medications and their metabolites into the environment causing major problems in the ecosystems [4]. Antibiotics are a type of important antimicrobial drug used to treat many human and animal diseases [5–7]. A few studies have been done on the evaluation of antibiotic use [8]. According to those studies, about 100–200

* Corresponding author.

thousand tons of antibiotics are consumed each year in the world and this amount is rising in recent years [9–11]. In addition, about 30%–90% of the taken drugs are redundant or not completely metabolized in the cells of human and animals bodies [12]. Antibiotics are non-biodegradable and remain in the environment for a long time because they are not eliminated by the common processes of wastewater treatment [13–16]. Thus, these pollutants enter the water resources through water treatment plants and reduce their quality, which have an undesirable effect on human health and living organisms [16–19]. Among the different types of antibiotics, tetracycline (TC) is the second most important group produced and consumed in the world [20,21]. There are many techniques for TC degradation such as electrochemistry, adsorption, and photo-catalysis [22–24]. In recent years, the application of advanced oxidation processes (AOPs) has shown to be very effective for drug removal [25]. AOPs refers to processes in which free hydroxyl radicals (OH^{\bullet}) are produced as oxidants in the degradation of hard and non-biodegradable organic matter [26,27]. Some pollutants directly absorb UV light and their chemical bonds are destroyed, while other substances are not decomposed rapidly or effectively by direct photolysis. As a result, hydrogen peroxide (H_2O_2) needs to be added to make the process more efficient [28,29]. Nowadays, the application of nanoparticles as catalysts with UV/ H_2O_2 has been proposed to remove drug pollutants due to process improvement, shortening of the purification steps, and safe production of by-products [30,31]. Among various catalysts and photo-catalysts, titanium dioxide (TiO_2) has been widely studied and used for the degradation of organic matter due to its high oxidation ability, physical and chemical stability, non-toxic nature, low cost, and high reactivity [32–37]. Since the UV/ H_2O_2 / FeNi_3 @ SiO_2 @ TiO_2 process with TiO_2 -NPs is a heterogeneous reaction, the retrieval of nanoparticles for reuse will need filtration or centrifugation processes. So far, several studies have shown that coating these nanoparticles with magnetic materials is one of the most effective and easy procedures for the recycle and reuse of the catalysts [38,39]. For example, FeNi_3 is a magnetic material used in the synthesis of nanoparticles as the nucleus of the catalysts due to its high magnetism [40]. So, the combination between FeNi_3 and TiO_2 nanoparticles, which is the focus of the present study, is one of the potential nanomaterials suggested by several studies as a catalyst in the photo-catalytic reactions for the eradication of organic pollutants in wastewater [41]. However, although FeNi_3 can absorb light, it does not contribute to the photo-catalysis [42]. Since FeNi_3 nanoparticles are highly reactive, they are simply oxidized and lose their magnetic properties. Also, some studies have shown that the application of iron compounds such as FeNi_3 and Fe_3O_4 would reduce the efficiency of photo-catalytic reactions due to the quenching of electrons by their surface defects [42,43]. Therefore, one of the ways to protect FeNi_3 is to use an impervious coating [44]. For this purpose, silica (SiO_2) can be utilized, thereby forming FeNi_3 @ SiO_2 . Therefore, FeNi_3 particles as the magnetic core and TiO_2 -NPs as the photo-catalytic shells were considered in the present study. These nanoparticles can be removed easily from the solutions by applying a magnetic force. The existence of a silica layer (SiO_2) between the outer shell (TiO_2) and the magnetic

core (FeNi_3), to form a novel FeNi_3 @ SiO_2 @ TiO_2 magnetic nanocomposite catalyst is essential to prevent the destruction of the magnetic core by simulated sunlight radiation as well as for the protection of the magnetic core against oxidation [44]. Hence, the objective of this work was firstly to synthesize and characterize a novel FeNi_3 @ SiO_2 @ TiO_2 magnetic nanocomposite. Later, the practical application of the synthesized catalyst for the degradation of TC using simulated sunlight in a laboratory UV/ H_2O_2 / FeNi_3 @ SiO_2 @ TiO_2 reactor was comprehensively studied.

2. Materials and methods

2.1. Reagents and chemicals

All chemicals were of analytical purity grade. Nickel chloride: $\text{NiCl}_2(6\text{H}_2\text{O})$, hydrazine hydrate: $\text{N}_2\text{H}_4\cdot\text{H}_2\text{O}$, titanium butoxide solution: $\text{C}_{16}\text{H}_{36}\text{O}_4\text{Ti}$, tetraethyl orthosilicate: $\text{SiC}_8\text{H}_{20}\text{O}_4$, iron chloride: $\text{FeCl}_2\cdot 4\text{H}_2\text{O}$, polyethylene glycol: $\text{HO}(\text{C}_2\text{H}_4\text{O})_n\text{H}$, ethanol, ammonia, and 1-Propanol were purchased from Merck Company (Germany). TC in powder form (chemical formula: $\text{C}_{22}\text{H}_{24}\text{O}_8\text{N}_2\cdot\text{HCl}$, molecular weight: 480.9 g/mol, solubility: 0.041 mol/L, and purity: 95%) was obtained from Sigma-Aldrich Co., (Germany) (Fig. 1). All solutions were prepared in distilled water and stored in opaque glass containers at 4°C for a maximum of 1 week. The pH values of the samples were adjusted by addition of 1 M HCl or 1 M NaOH during the experiments (Merck, Germany).

2.2. Catalyst synthesis

In Fig. 2, a general scheme of the FeNi_3 @ SiO_2 @ TiO_2 nanocomposites synthesis is presented. The synthesis steps of the FeNi_3 @ SiO_2 @ TiO_2 nanoparticles were as follows.

To synthesize the FeNi_3 @ SiO_2 @ TiO_2 magnetic nanoparticles the co-precipitation and sol-gel methods were used [40]. First, 1.00 g of $\text{HO}(\text{C}_2\text{H}_4\text{O})_n\text{H}$ was dissolved in 180 mL of deionized water. Then, 10 mL of two diverse solutions containing 0.188 g of $\text{FeCl}_2\cdot 4\text{H}_2\text{O}$ and 0.713 g of $\text{NiCl}_2\cdot 6\text{H}_2\text{O}$, were prepared and further added simultaneously into the previous solution. The pH of the resulting solution was adjusted between 12 and 13 by the addition of NaOH. In the next step, the resultant mixture was stirred with 1.9 mL of $\text{N}_2\text{H}_4\cdot\text{H}_2\text{O}$ for 24 h. Eventually, the synthesized FeNi_3 nanoparticles were separated from the mixture by an external magnetic field, rinsed by deionized water, and dried at 80°C in a vacuum oven. Thereafter, the synthesized FeNi_3 magnetic nanoparticles were reacted with SiO_2 to obtain FeNi_3 @ SiO_2 shell-core nanoparticles. For this, 0.5 g of the FeNi_3 nanoparticles was dissolved in a mixture prepared by dissolving 20 mL of distilled water, 80 mL of ethanol and 2 mL of ammonia. Next, 1 mL of $\text{SiC}_8\text{H}_{20}\text{O}_4$ solution was added slowly to the previous mixture under shaking (500 rpm for 24 h) using a stirrer (model Alpha D500). Finally, the SiO_2 @ FeNi_3 magnetic nanoparticles obtained were separated *via* an external magnetic source, washed with ethanol and distilled water and then placed at 60°C in a vacuum oven until dried. For the synthesis of FeNi_3 @ SiO_2 @ TiO_2 , 0.2 g of the prepared FeNi_3 @ SiO_2 nanoparticles was dissolved in 50 mL of distilled water. Two mL of $\text{C}_{16}\text{H}_{36}\text{O}_4\text{Ti}$ solution was

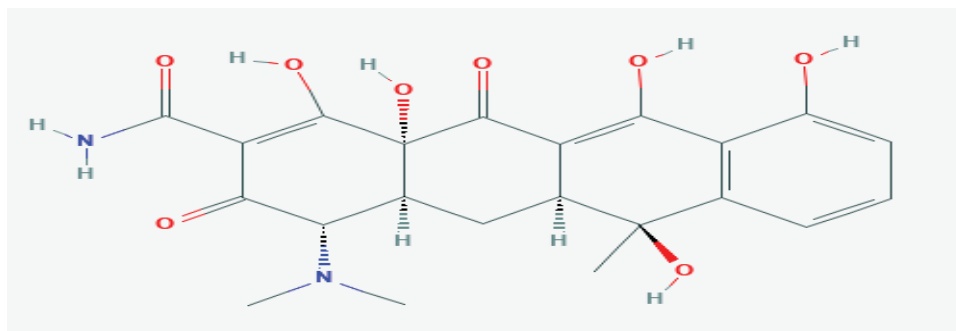
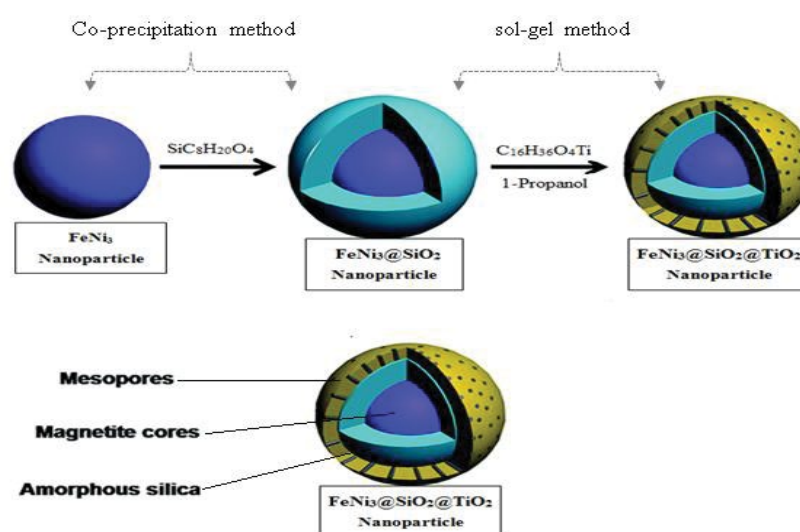


Fig. 1. Structural formula of TC.

Fig. 2. Schematic diagram of synthesizing steps of $\text{FeNi}_3@SiO_2@TiO_2$ magnetic nanocomposite.

mixed with 10 mL of 1-propanol and added drop-wisely into the previously prepared $\text{FeNi}_3@SiO_2$ solution. Subsequently, the solution was placed in a shaker incubator at 500 rpm and 80°C (Model SI-100R, Korea). The suspension was left to cool down and the resulting solid material of $\text{FeNi}_3@SiO_2@TiO_2$ was separated using a magnet. Afterwards, the collected $\text{FeNi}_3@SiO_2@TiO_2$ nanoparticles were firstly washed in ethanol, then in distilled water, and dried at a temperature of 30°C until there was no moisture content. Finally, the $\text{FeNi}_3@SiO_2@TiO_2$ nanoparticles were calcined (400°C, for a maximum period of 5 h), to remove any organic matter and used as a template in the structure of the nanoparticles.

2.3. Characterization analysis

Structural characteristics and surface morphology of the synthesized $\text{FeNi}_3@SiO_2@TiO_2$ nanoparticles were determined with different advanced techniques. The morphological characteristics of nanoparticles individually and in combination were investigated by applying high resolution micrographs captured at different magnifications by transmission electron (TEM) and field emission-scanning electron (FE-SEM) microscopies whose specifications were Zeiss-EM10C-100 KV and ZEISS-Sigma-500 scanners (Germany),

respectively. In order to identify the type of functional groups, Fourier transform infrared (FTIR) spectroscopy was applied at 4,000 to 400 cm^{-1} wavenumber range, where the FTIR spectra were obtained using an AVATAR FTIR spectroscopy (USA). For the determination of the particle crystalline structure, an X-ray diffractometer (XPert Pro, PANalytical Co., Netherland) with high power $\text{CuK}\alpha$ radiation maintained at a scan rate of 2°/min was used. Vibrating sample magnetometer (VSM) techniques (Lake Shore-7404, USA) were applied to determine the magnetic force of the FeNi_3 , $\text{FeNi}_3@SiO_2$, and $\text{FeNi}_3@SiO_2@TiO_2$ nanoparticles at a temperature of 300K. Also, to identify the elemental distribution of $\text{FeNi}_3@SiO_2@TiO_2$ magnetic nanocomposite, a Shimadzu energy-dispersive X-ray spectroscopy (EDS, EDX-700HS, Japan) was utilized.

2.4. $\text{FeNi}_3@SiO_2@TiO_2/UV/H_2O_2$ experiments and performance evaluation

In this paper, all experiments were performed in a reactor (Fig. 3) with a capacity of 500 mL in the presence of tetracycline (TC) and $\text{FeNi}_3@SiO_2@TiO_2$ magnetic nanoparticles. A mercury UV-lamp (Toshiba, Japan) was installed in the center of the reactor for supplying a uniform UV

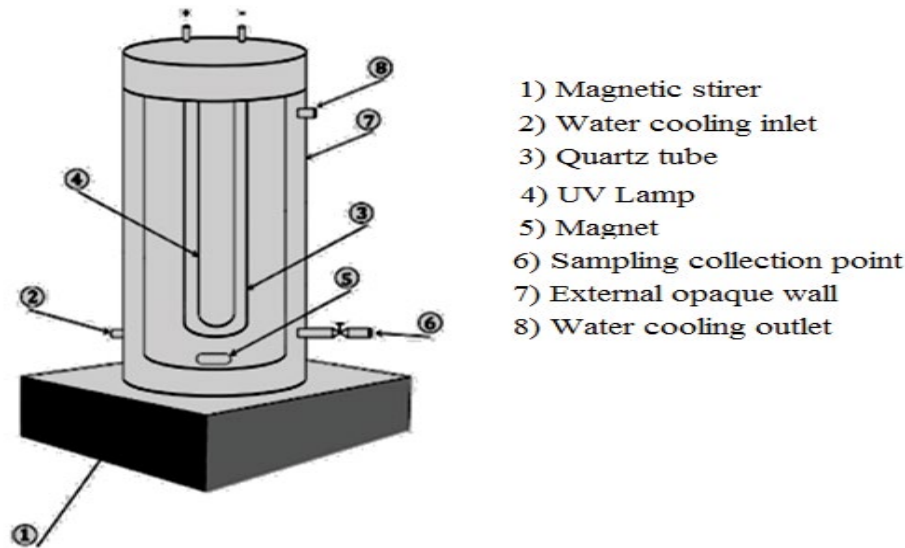


Fig. 3. Schematic of the UV/H₂O₂/FeNi₃/SiO₂/TiO₂ reactor.

irradiation of an intensity of 2,500 μW/cm² and a wavelength of 358 nm throughout the reactor. The TC degradation was examined under magnetic stirring (500 rpm), a temperature of 20°C ± 2°C, initial TC concentrations ranging from 10 to 30 mg/L, amount of FeNi₃@SiO₂@TiO₂ nanoparticles from 0.005 to 0.1 g/L, pH of the TC solutions from 3 to 9, a contact time up to 180 min and H₂O₂ concentrations from 50 to 200 mg/L. In order to prevent interference and effects of other light sources such as the visible light, all working TC solutions were kept in the dark until used. At different times of reaction, 2 mL of TC solution was collected, centrifuged to separate the catalyst nanoparticles from the solution, and finally, the residual concentration of TC in the solution was determined. All TC concentrations were measured by a UV/Vis spectrometer at a wavelength of 358 nm. Each sample was analyzed thrice, and the mean value was calculated in all degradation experiments. In order to evaluate the effect of tetracycline removal by the UV/H₂O₂/FeNi₃@SiO₂@TiO₂ reactor, the efficiency ratios of non-degraded (C_t) and initial (C₀) concentrations were determined. Notably, the evolution curves obtained from the study of the effect of the reaction time at different initial TC concentrations on the degradation process were subsequently applied for the kinetics study.

2.5. Kinetics study

In order to evaluate the degradation performance of the catalyst used to remove organic pollutants in oxidation processes such as photo-catalysis and FeNi₃@SiO₂@TiO₂/UV/H₂O₂ processes, it is essential to determine the kinetics mechanism. For this purpose, the most common kinetics model which is applicable in the modeling of the degradation data of organic materials is the Langmuir–Hinshelwood model [45]. In the case of very low pollutant concentration, the Langmuir–Hinshelwood formula can be rewritten in the form of a first-order equation, which is illustrated in its simplified linear form in Eq. (1). The accuracy of the fitting

between the applied kinetics models and the experimental data was evaluated according to the resulting values of the regression coefficient (R²).

$$\ln\left(\frac{C_t}{C_0}\right) = -k_a t \quad (1)$$

In this equation, k_a represents the reaction rate of the first-order (min⁻¹), and C_t stands for the TC concentration (mg/L) measured at the irradiation time (t , min).

2.6. Catalytic reusability experiments

To investigate the reusability of the FeNi₃@SiO₂@TiO₂ nanoparticles as catalysts, the experimental tests of TC photocatalytic degradation were carried out for four consecutive cycles under the obtained optimum conditions (i.e., pH=5, TC concentration=20 mg/L, reaction time=90 min, FeNi₃@SiO₂@TiO₂ dose = 0.1 g/L). At the end of each process, the nanoparticles were removed by applying an external magnetic field, washed with distilled water, and then dried in an oven at 80°C in order to use it in the next cycle.

3. Results and discussion

3.1. Magnetic nano-particles characterizations

3.1.1. FTIR spectrum

FTIR analysis is one of the common analyses applied to investigate the type of bonds and functional groups in the structure of a compound. The FTIR spectrum of FeNi₃/SiO₂/TiO₂ nanocomposite is shown in Fig. 4. The weak peaks at 1,032 and 913.61 cm⁻¹ are associated with the Ti–O–S bending vibrations [46,47]. The absorption peaks at the range from 531.57 to 1,031.52 cm⁻¹ belong to the vibration bonding of Ti–O–Ti. The bands around 3,382.97 and 1,621.79 cm⁻¹ are attributed to the stretching and bending of O–H bonds.

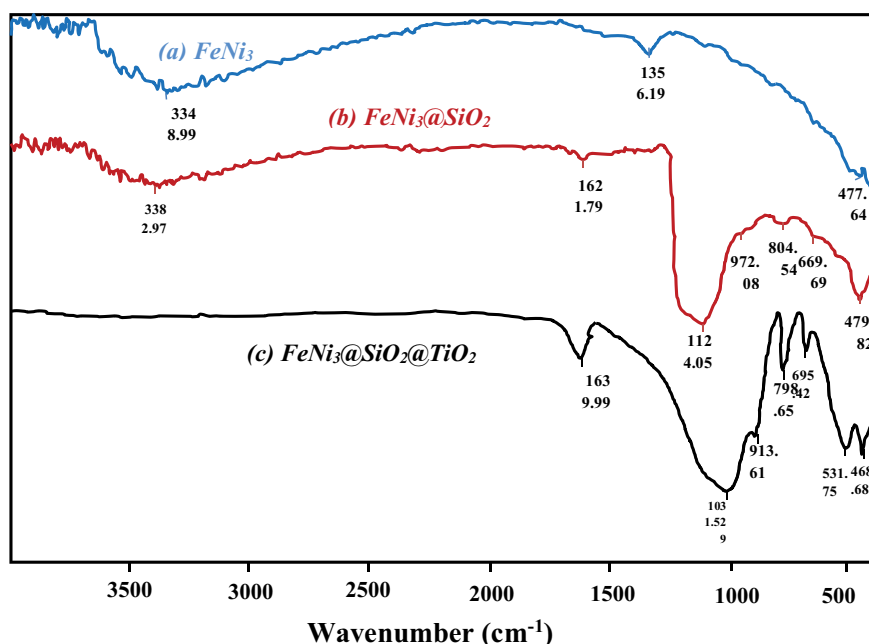


Fig. 4. FTIR spectra of (a) FeNi₃, (b) FeNi₃@SiO₂, and (c) FeNi₃@SiO₂@TiO₂ nanoparticles.

The peak at 800 cm⁻¹ corresponds to the symmetric vibration of Si–O–Si and the wavenumber of 1,080 cm⁻¹ originates from the asymmetric vibration of Si–O–Si.

On the other hand, the Fe–Ni bond can be responsible for the absorption peaks at 498.69 cm⁻¹ [48,49]. In a study conducted by Khodadadi et al. [40] on the synthesis of FeNi₃/SiO₂/TiO₂ nanocomposites, similar results were obtained.

3.1.2. XRD spectrum

In this work to determine the approximate size of FeNi₃/SiO₂/TiO₂ nanocomposite as well as to identify its structure, the XRD (X-ray diffraction) analysis was employed and the results are shown in Fig. 5. The presence of peaks at 75.5°,

51.7°, and 44.5° at 2θ represents the crystalline form of FeNi₃. The peak of 2θ = 10°–25° corresponds to silica material and indicates the existence of SiO₂ in the synthesized materials. The diffraction angles of 25.2°, 37.9°, 54.7°, and 63° indicate the existence of TiO₂ in the synthesized materials. The peak of amorphous SiO₂ at the diffraction angle of 22° is below the TiO₂ peak [40,44]. The crystallite size of nanoparticles and nanocomposites was calculated using the Debye–Scherrer formula whose mathematical relation is shown in Eq. (5). In that Eq. (5), the values of *D*, β, λ, and θ correspond to the crystallite size, the full width at half maximum of the peak corresponding to the plane (peak in 25.2°), the wavelength of XRD radiation and the angle obtained from 2θ value corresponding to the XRD pattern, respectively.

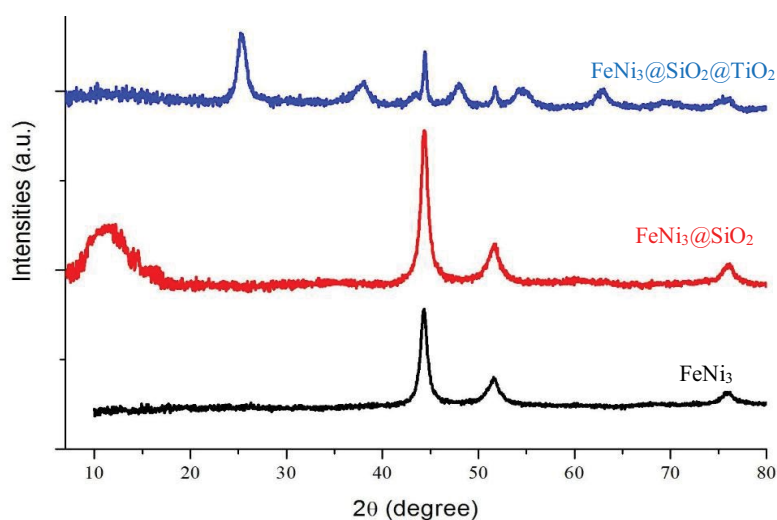


Fig. 5. XRD spectra of FeNi₃, FeNi₃@SiO₂, and FeNi₃@SiO₂@TiO₂ nanoparticles.

$$D = \frac{0.98\lambda}{\beta \cos\theta} \quad (2)$$

By applying the Debye–Scherer equation, the mean crystallite size of FeNi₃ nanoparticles, FeNi₃/SiO₂ and FeNi₃/SiO₂/TiO₂ nanocomposites were found to be 10, 12, and 77 nm, respectively.

3.1.3. SEM image

To survey the structure and size of the synthesized magnetic nanocomposite, the FE-SEM was used and the obtained result is shown in Fig. 2. According to Fig. 6, the FeNi₃/SiO₂/TiO₂ nanocomposites had a high density and the reason for that was their magnetic properties. Also, according to Fig. 2, the nanocomposites had an irregular shape.

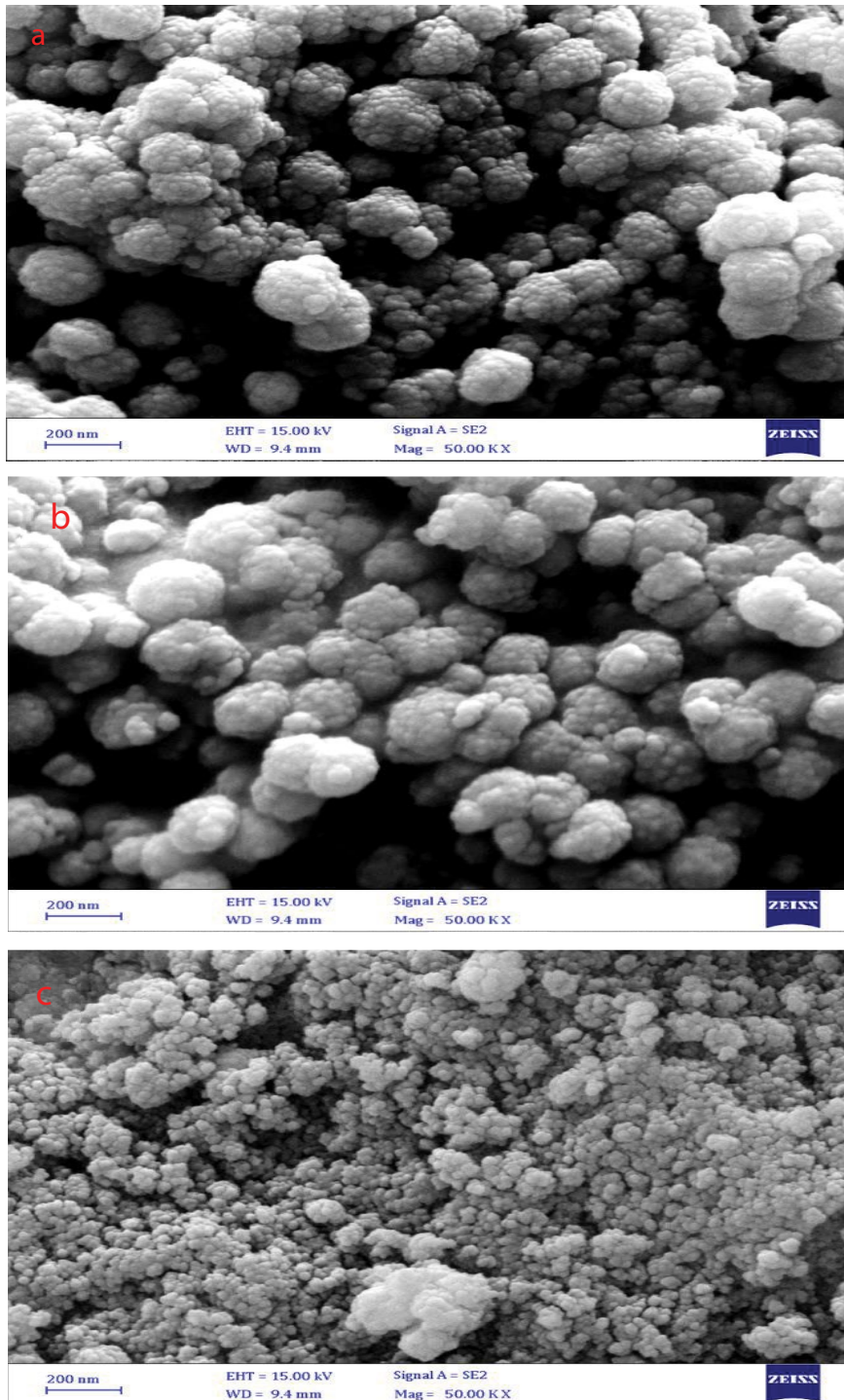


Fig. 6. FE-SEM images of FeNi₃ (a), FeNi₃@SiO₂ (b), and FeNi₃@SiO₂@TiO₂ (c) nanoparticles.

Moreover, it could be noticed that the coating processes of FeNi_3 surface with SiO_2 and then with TiO_2 , did not destroy or alter the morphological structure of the FeNi_3 . It was apparent from the FE-SEM image of the $\text{FeNi}_3@/\text{SiO}_2/\text{TiO}_2$ nanoparticles that their surface was coarse and their shape was uniformly spherical with a diameter in the range of 20–30 nm. According to IUPAC (International Union of Pure and Applied Chemistry), the synthesized $\text{FeNi}_3/\text{SiO}_2/\text{TiO}_2$ nanocomposites were mesoporous [40].

3.1.4. TEM image

TEM analysis is considered a special method to determine the structure and morphology of materials since it enables to study of material microstructures with high magnification and resolution. The result of TEM analysis is shown in Fig. 7. According to Fig. 3, the outer light shell of the TEM image of $\text{SiO}_2/\text{FeNi}_3$ is the coating layer of SiO_2 while the inner bold core represents the FeNi_3 . Also, the TEM image of $\text{FeNi}_3@/\text{SiO}_2/\text{TiO}_2$ showed that these

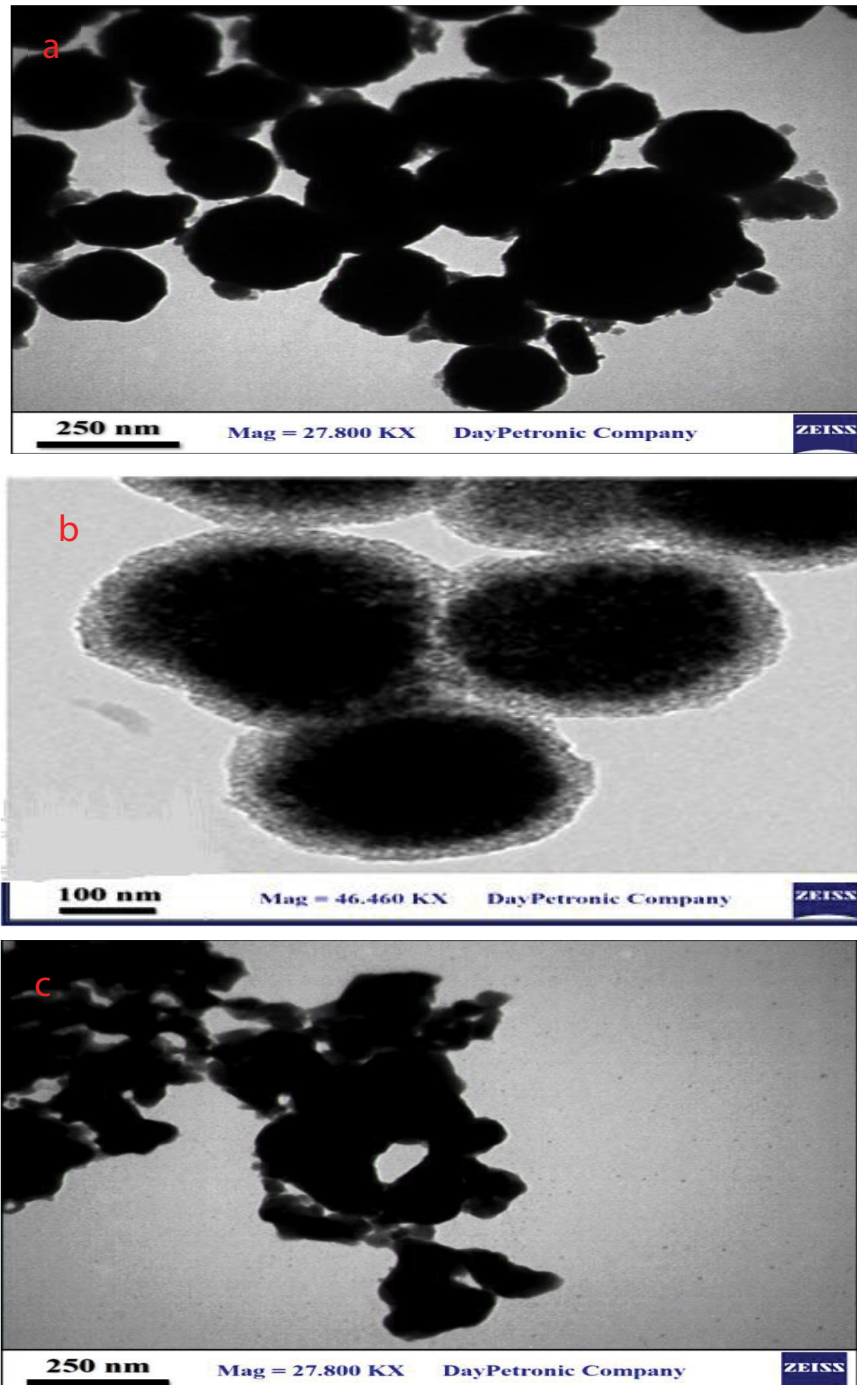


Fig. 7. TEM images of FeNi_3 (a), $\text{FeNi}_3/\text{SiO}_2$ (b), and $\text{FeNi}_3/\text{SiO}_2/\text{TiO}_2$ (c) nanoparticles.

nanoparticles were multi-dispersed and thus, their agglomeration was high.

3.1.5. VSM technique

In this study, Hysteresis loop analysis was applied to investigate the magnetic properties of the synthesized nanocomposites. The magnetic properties of FeNi₃ nanoparticles and the synthesized nanocomposites FeNi₃/SiO₂ and FeNi₃/SiO₂/TiO₂ were investigated by a VSM instrument at a temperature of 300 K and the obtained results are shown in Fig. 8. According to the VSM results FeNi₃ nanoparticles, FeNi₃/SiO₂ nanocomposite, and FeNi₃/SiO₂/TiO₂ nanocomposite had saturation magnetizations of 68.52, 58.99, and 18.84 emu/g, respectively. It was observed that the magnetic properties of FeNi₃ core were reduced with increasing cover layers on it. Anyway, it was possible to collect the nanoparticles in the presence of an external magnetic field [40].

3.1.6. Energy-dispersive X-ray technique

In the current research to determine the abundance of specific elements, EDS and EDX (energy-dispersive X-ray spectroscopy) analysis was applied to the synthesized magnetic nanocomposites. The EDS analysis is used to find the chemical composition of materials down to a spot size of a few microns. The results of the EDS analysis of the FeNi₃/SiO₂/TiO₂ nanocomposites are shown in Fig. 9. According to this analysis, the area of the peaks corresponds to the elements in the material structure. As is clear from the EDX, the elements of Ti, O, Ni, Fe, and Si were present in the structure of the synthesized nanocomposites with a mass percent of 41.9%, 31.6%, 19.5%, 5.9%, and 1.1%, respectively.

3.1.7. Thermal gravimetric analysis technique

In thermal gravimetric analysis (TGA) or thermo-gravimetric analysis the mass of a sample is measured along

time as the temperature changes. This technique provides information about physical and chemical phenomena such as thermal decomposition and chemisorption. The results of TGA analysis of the FeNi₃/SiO₂/TiO₂ nanoparticles are shown in Fig. 10. The first weight loss (weight decreased about 3.26%) occurred at 50°C and the reactions were endothermic because the temperature changes were negative. These changes were probably due to the extraction of volatile solvents with low boiling point. In addition, the second weight loss (weight decreased about 0.05%) was observed at a temperature of 650°C. This temperature is the state at which the sample gradually enters the phase change. It should be noted that due to the high melting and boiling points of the sample, the element in the FeNi₃/SiO₂/TiO₂ nanoparticles structure was not extracted in the synthesized sample.

3.2. Effects study

In UV/H₂O₂/FeNi₃@SiO₂@TiO₂ process, the type of chemical reactions as well as the surface properties of the pollutant molecules and catalyst particles is significantly affected by the environmental conditions. So, experiments were carried out to determine the effect of pH, initial TC concentration, H₂O₂ concentration, and catalyst nanoparticle dose on TC degradation efficiency using FeNi₃@SiO₂@TiO₂ nanoparticles [50].

3.2.1. Effect of pH on TC degradation

pH is one of the most important factors that can influence chemical processes such as UV/H₂O₂/FeNi₃@SiO₂@TiO₂ reaction [51,52]. This is due to this parameter can change the surface charge of the utilized catalyst as well as its properties. Besides that, it can also affect the mechanism of radical hydroxyl production, reaction kinetics, and contaminant structure [53]. In the current study, the effect of pH on the performance of TC degradation was investigated

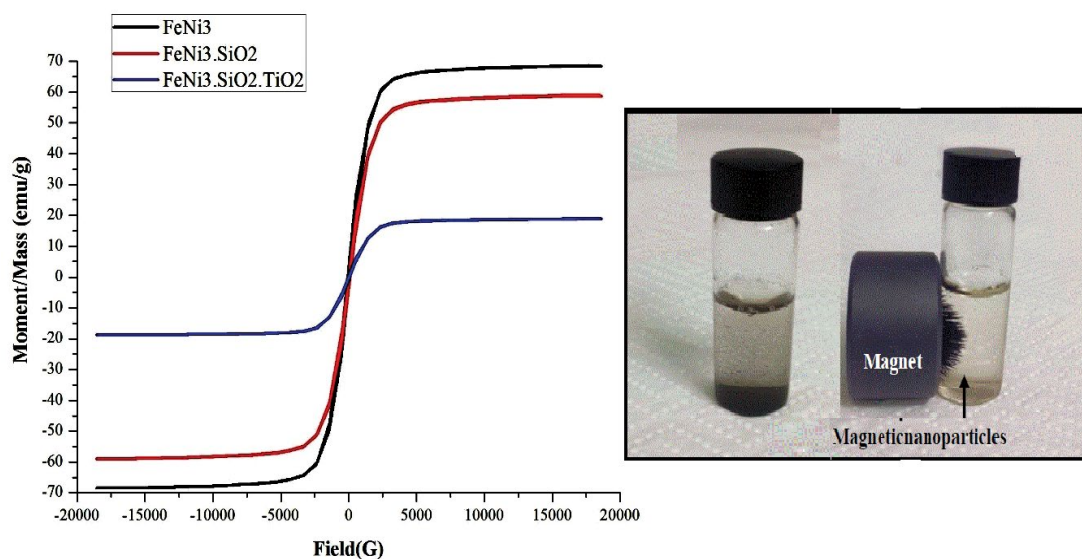


Fig. 8. VSM analysis of FeNi₃, FeNi₃/SiO₂, and FeNi₃/SiO₂/TiO₂ nanoparticles.

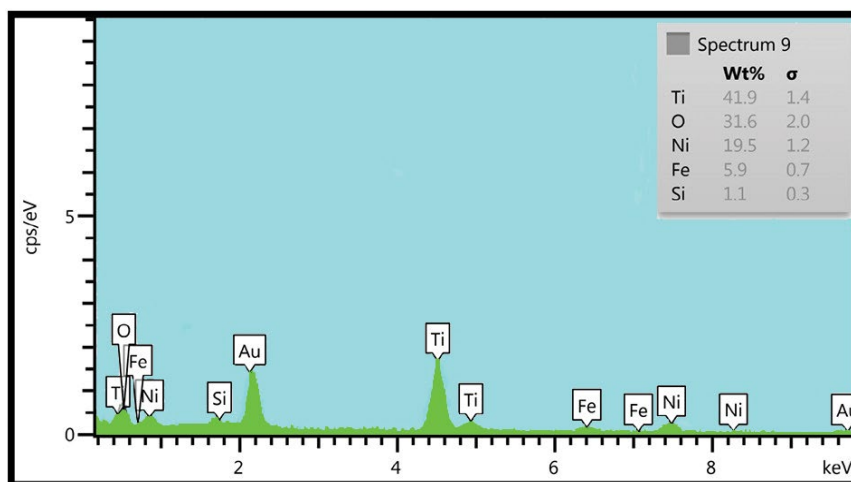


Fig. 9. EDS spectrum of $\text{FeNi}_3\text{@SiO}_2\text{@TiO}_2$ nanoparticles.

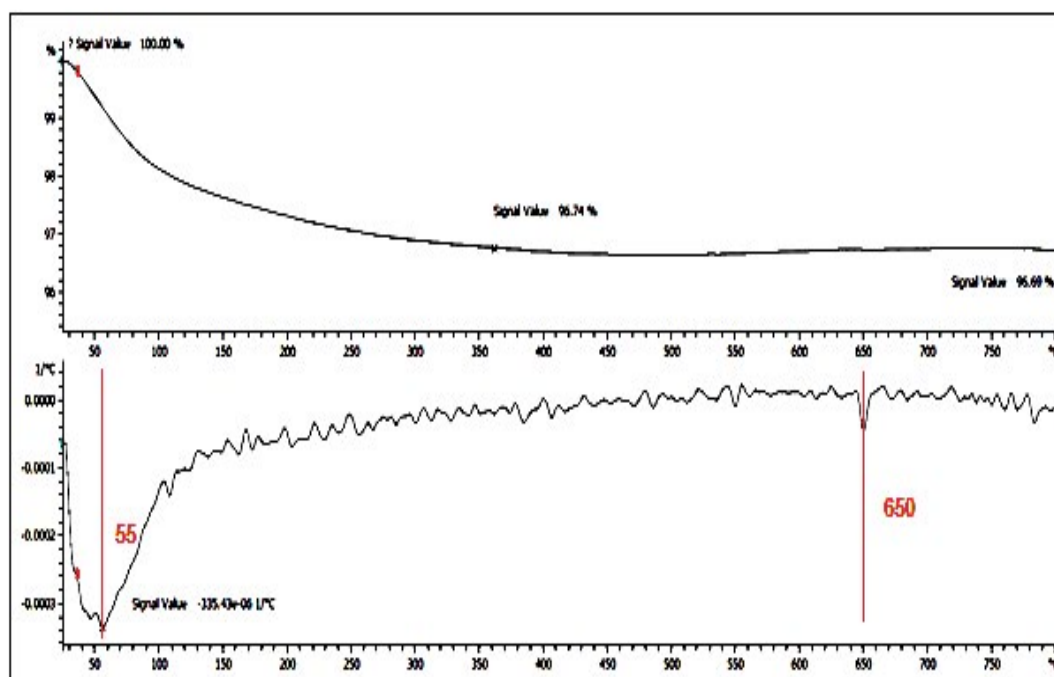


Fig. 10. TGA analysis of $\text{FeNi}_3\text{@SiO}_2\text{@TiO}_2$ nanoparticles.

from 3 to 9 (Fig. 11), while keeping the other experimental factors fixed (i.e., TC concentration = 20 mg/L, catalyst dose = 0.02 g/L, reaction time = 200 min, and H_2O_2 concentration = 150 mg/L). According to the obtained results (Fig. 11a), the highest removal efficiency (100%) was achieved at pH = 5. Above this pH, TC degradation decreased (Fig. 11). The pH changes can influence the adsorption of TC onto the nanocomposite surfaces. Thus, according to the pH value of the solution, various TC species will predominate (Fig. 1). At $\text{pH} < 3.30$ (pKa_1), TC molecules will be mainly present as fully protonated H_4TC^+ , while at $3.30 < \text{pH} < 7.68$ (pKa_2), most TC molecules will occur as neutral H_3TC^0 species. In addition, at $7.68 < \text{pH} < 9.70$ (pKa_3) TC will exist as H_2TC^- and at $\text{pH} > 9.70$ the TC^{2-} will be the predominant

species of the TC molecules [40]. Furthermore, to determine the catalyst's surface charge, one of the methods is the pH_{pzc} analysis. The analysis of point of zero charge (pzc) determination showed that the $\text{FeNi}_3\text{@SiO}_2\text{@TiO}_2$ nanoparticles pH_{pzc} was nearly 6.2 (Fig. 11b). Thus, above the pH_{pzc} value, the surface of the prepared catalyst will be saturated by the negative charges of the surplus OH^- ions and pH_{pzc} . Thus, the dominant $\text{FeNi}_3\text{@SiO}_2\text{@TiO}_2$ functional groups of negative charges may get protonated by H^+ protons, so in acidic pH the catalyst surface was positively charged.

The nanoparticle surface load and TC were negatively charged in alkaline pH and, thus, the repulsive force between them increased [54]. In addition, TC antibiotic exists molecularly at pHs between 3.3 and 7.68, which is suitable

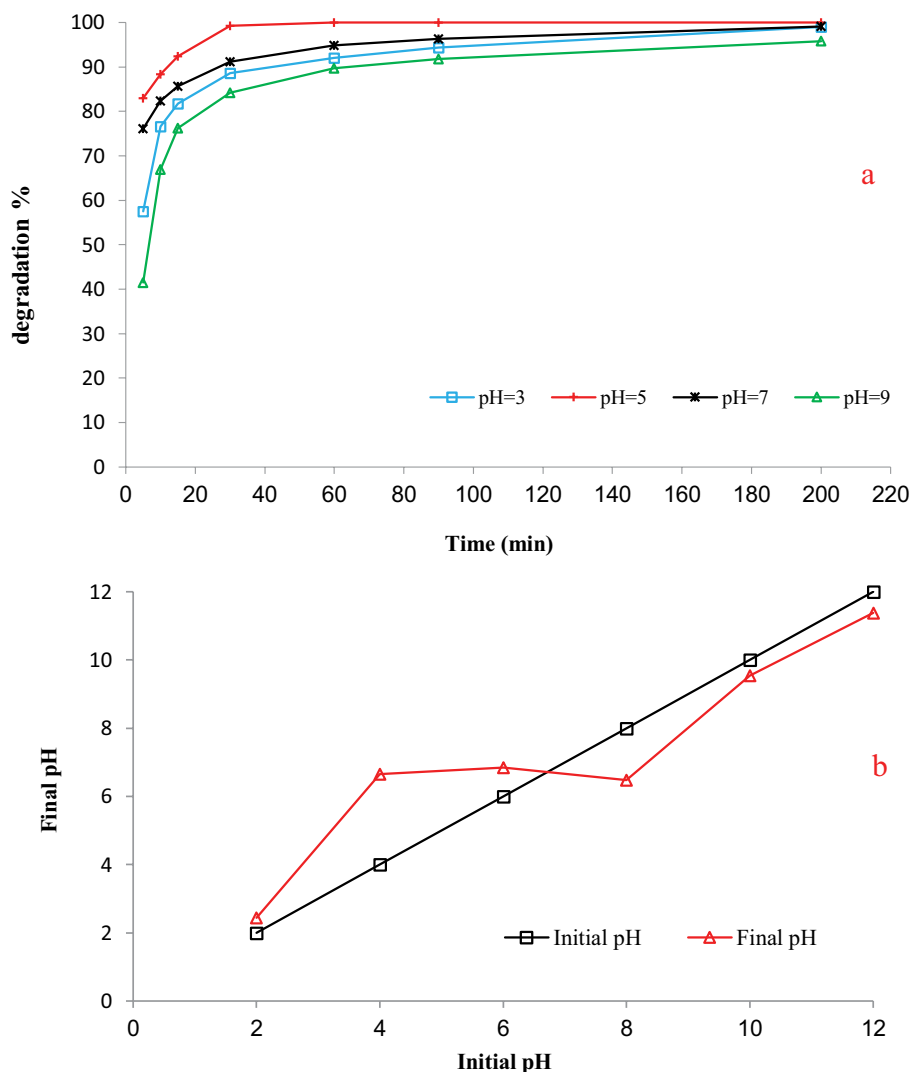


Fig. 11. Plots of the results of pH effect (a) and the results of pH_{zpc} (b).

for TC adsorption, and due to nanoparticle and TC surface loads, the $\text{UV}/\text{H}_2\text{O}_2/\text{FeNi}_3@\text{SiO}_2@\text{TiO}_2$ reaction improves [55]. At low pHs, the positive binding sites are the main cause of TC degradation, and the high oxidation of TC can be due to the hydrolysis of this contaminant. Besides that, H_2O_2 is an oxidizing agent but is not active under normal environmental conditions and, therefore, it requires an activation agent such as ultrasonic, UV light, catalyst, or heat [54]. In this study, UV radiation was the activation agent of H_2O_2 which was used to produce free radicals and ultimately improve the $\text{UV}/\text{H}_2\text{O}_2/\text{FeNi}_3@\text{SiO}_2@\text{TiO}_2$ process through further oxidation of TC. Rasheed et al. [56] applied $\text{MIL-100}(\text{Fe})@\text{Fe}_3\text{O}_4/\text{CA}$ magnetic nano-photo-catalysts for TC degradation by a Fenton-like process and the results were indicated that the highest efficiency was obtained at $\text{pH} = 5$.

3.2.2. Effect of catalyst dose on TC degradation

From an economic perspective, the determination of an optimum catalyst dose is one of the important parameters

that should be found before applying the $\text{UV}/\text{H}_2\text{O}_2/\text{FeNi}_3@\text{SiO}_2@\text{TiO}_2$ treatment method. The effect of the variation of $\text{FeNi}_3@\text{SiO}_2@\text{TiO}_2$ nanoparticles on the TC removal process was investigated within the range from 0.005 to 0.1 g of catalyst particles at $\text{pH} = 5$, reaction time up to 200 min, initial TC concentration = 20 mg/L and H_2O_2 concentration = 150 mg/L. The results revealed that by increasing the catalyst dose from 0.005 to 0.01 g/L, the degradation percentage of TC increased. However, TC degradation decreased at higher doses, so that in 60 min the percentage of TC removal was reduced from 100% to 80.58% for a catalyst dose of 0.01 and 0.1 g/L, respectively. Thus, the highest TC degradation efficiency was observed at a catalyst dose of 0.01 g/L (Fig. 12). This can be explained by the increase of the solution turbidity with the increase of the catalyst dose, which will hinder the penetration of the UV radiation, thereby decreasing the degradation rate of TC [53,57,58]. Additionally, the occurrence of the agglomeration of some catalyst nanoparticles at high doses in the solution could also be the reason for a decrease in the percentage of

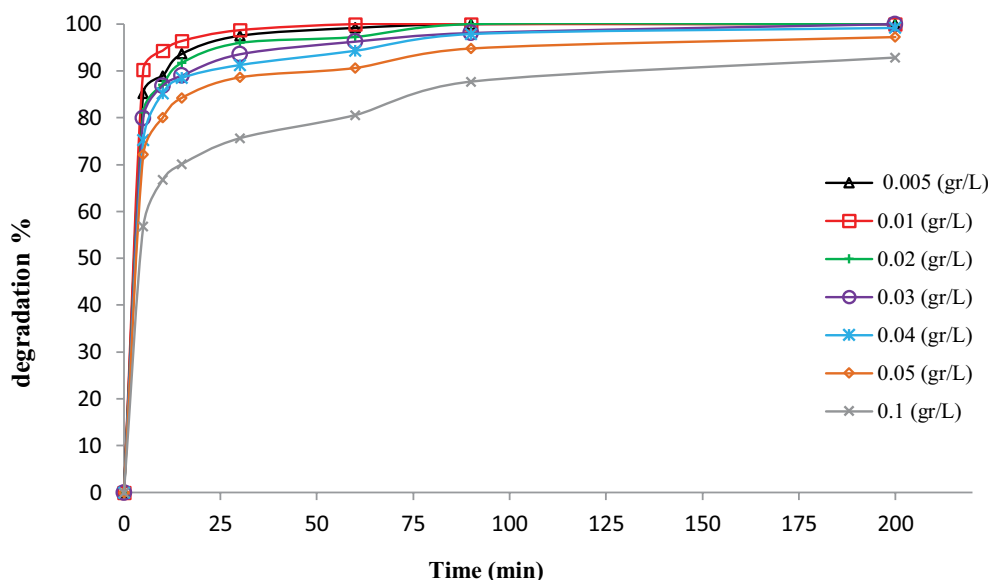
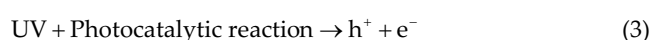


Fig. 12. Plots of the results of the nanocomposite effect.

TC degradation. Another reason for the decrease of TC degradation by increasing the amount of catalyst in the reactor is the increase of the reaction sites for the contaminant, also the absorbed UV radiation by the nanoparticles is elevated, that ultimately enhance the production of the high reactive radicals that ready for degradation reaction of pollutants [59]. Simultaneously, this process will lead to the generation of more free electrons ready to react with water molecules and dissolved oxygen in the solution and produce highly reactive radicals (i.e., OH^\bullet and $\text{O}_2^{\bullet-}$), which are essential to promote the $\text{UV}/\text{H}_2\text{O}_2/\text{FeNi}_3@\text{SiO}_2@\text{TiO}_2$ activity towards organic molecules, as illustrated by the chemical reaction Eqs. from (2) to (9) [41].



3.2.3. Effect of TC concentration on TC degradation

The initial concentration of the pollutant is another affecting factor on the efficiency of the $\text{UV}/\text{H}_2\text{O}_2/\text{FeNi}_3@\text{SiO}_2@\text{TiO}_2$ process. In this study, the effect of the TC concentration from 10 to 30 mg/L was investigated on the $\text{UV}/\text{H}_2\text{O}_2/\text{FeNi}_3@\text{SiO}_2@\text{TiO}_2$ process while keeping the other experimental parameters fixed at their optimal values obtained in previous tests. According to the obtained results, increasing the TC concentration from 10 to 30 mg/L led to a reduction in the process efficiency from 100% to 89.1% for a reaction time of 60 min (Fig. 13). This could be due to lower concentrations of TC, there are more available sites on the surface of the nano-catalyst for TC adsorption. But increasing the concentration of TC will lead to a decrease in the available sites on the surface of the catalyst for TC adsorption. But the mean reason for this trend may be related to the fact that the concentrations of radicals produced are the same in all solutions, therefore, the rate of decomposition is higher in the solution with a low concentration of TC. The obtained results are consistent with those reported by other researchers [40,44].

3.2.4. Effect of H_2O_2 concentration on TC degradation

Hydrogen peroxide is a powerful oxidizing agent used in oxidation hybrid processes. Since the number of hydroxide radicals produced is directly related to the degradation process, the percentage of degradation raises with the increasing concentration of hydrogen peroxide [53,60].

In the current study, the experiments were further performed to investigate the effect of H_2O_2 concentration (50–200 mg/L) on TC degradation in the $\text{FeNi}_3@\text{SiO}_2@\text{TiO}_2/\text{UV}/\text{H}_2\text{O}_2$ process while the other experimental parameters that affect the TC degradation mechanism such as pH, TC concentration and $\text{FeNi}_3@\text{SiO}_2$ catalyst dosage were fixed at their optimal values obtained in previous tests. The obtained results showed that increasing hydrogen

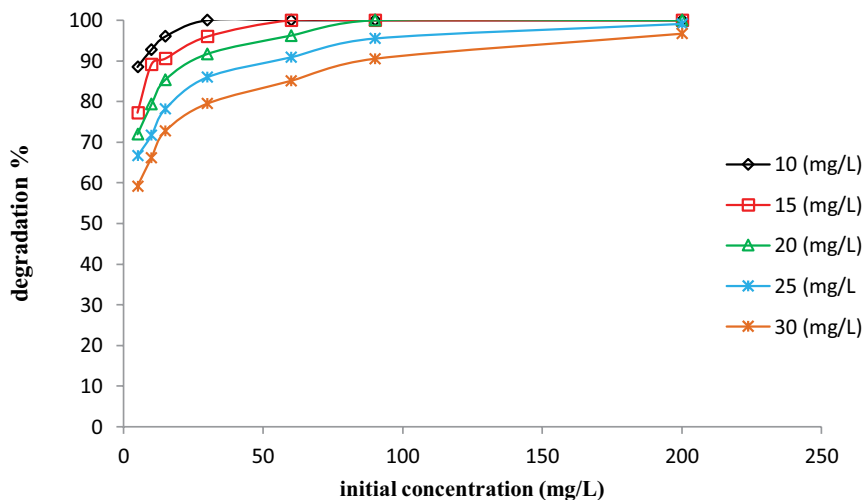


Fig. 13. Plots of the results of initial TC concentration effect.

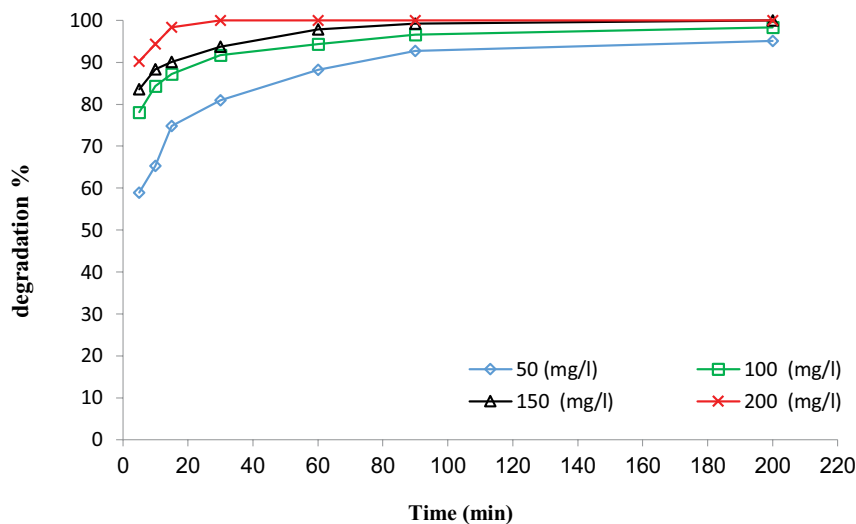


Fig. 14. Plots of the results of H_2O_2 concentration effect.

peroxide concentration led to an increase in TC degradation efficiency such that by increasing hydrogen peroxide concentration from 50 to 200 mg/L, TC degradation efficiency increased from 88% to 100% for a contact time of 60 min (Fig. 14). This could be attributed to the production of more oxidizing agents (OH^*) in the UV/ H_2O_2 /FeNi₃@SiO₂@TiO₂ process, which would result in the degradation of more TC molecules. In other words, hydrogen peroxide is an oxidizing agent and it is inactive in environmental conditions, but when affected by UV irradiation, H_2O_2 will be activated and the result is hydroxyl radical (OH^*) production [41]. In the study conducted by Shiraz et al. [51] the investigation of catechol degradation by persulfate activated by UV and ferrous ions led to similar results.

3.2.5. Kinetics study

In the chemical processes to evaluate the degradation rate of organic pollutants, calculating the reaction kinetics is

an important factor. The Langmuir–Hinshelwood model is used to describe the kinetics study and degradation rate of organic contaminants such as the TC antibiotic.

The results of the reaction kinetics study of the Langmuir–Hinshelwood model to describe the TC degradation process of UV/ H_2O_2 /FeNi₃/SiO₂/TiO₂ are shown in Fig. 15 and Table 1. Due to the obtained high R^2 values, a satisfactory agreement has been observed between the experimental data and the Langmuir–Hinshelwood model. Moreover, According to the obtained results the reaction rate constant (K_{obs}) significantly decreased by increasing the TC concentration, so that for an initial TC concentration of 10 mg/L K_{obs} was $256/9 \times 10^{-3} \text{ min}^{-1}$ and for an initial TC concentration of 30 mg/L, K_{obs} dropped to $21.4 \times 10^{-3} \text{ min}^{-1}$.

3.2.6. Reusability of FeNi₃@SiO₂@TiO₂ nanoparticles

The results of Fig. 16 illustrates the economic and operational capability of FeNi₃@SiO₂@TiO₂ nanoparticles through

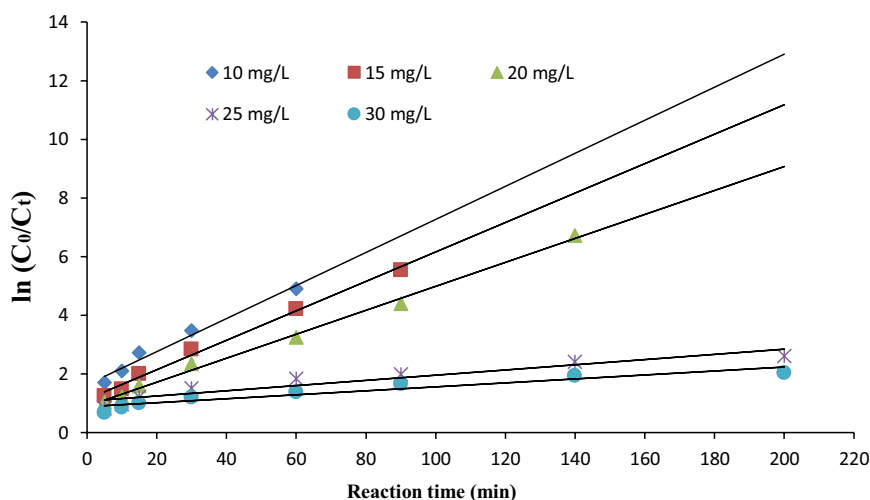


Fig. 15. Linear fitting of the kinetic data of TC degradation at different initial concentrations.

Table 1

Results of the modeling of experimental kinetic data of TC degradation with the pseudo-first-order equation

Initial TMX concentration (mg/L)	Equation where $Y = \ln\left(\frac{C_t}{C_0}\right)$ and $x = t$	k_a (1/min)	$t_{1/2}$ (min)	R^2
10	$Y = 0.256x + 1.6323$	256×10^{-3}	2.71	0.9765
15	$Y = 0.099x + 1.1387$	99×10^{-3}	7.00	0.9921
20	$Y = 0.052x + 0.9008$	52.8×10^{-3}	13.125	0.9951
25	$Y = 0.041x + 1.0702$	41.4×10^{-3}	16.74	0.9533
30	$Y = 0.021x + 0.883$	21.4×10^{-3}	32.38	0.9650

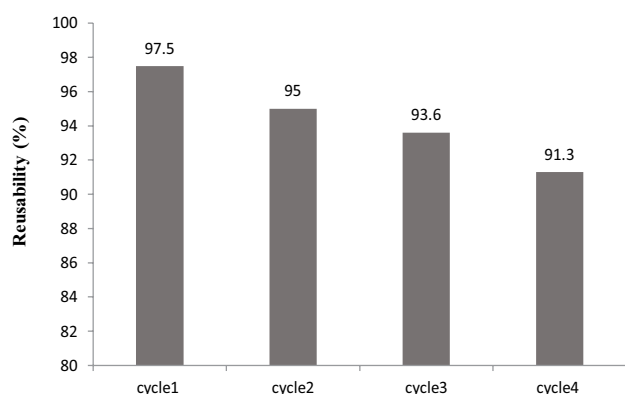


Fig. 16. Reusability percentage of $\text{FeNi}_3\text{@SiO}_2\text{@TiO}_2$ magnetic nanocomposite.

sustainability and reusability experimental tests. The achieved results demonstrated a very low reduction of $\text{UV}/\text{H}_2\text{O}_2/\text{FeNi}_3\text{@SiO}_2\text{@TiO}_2$ nanoparticles activity at the end of each cycle. Thus, only 10% of nanoparticle activity dropped after four consecutive cycles. This reveals that $\text{FeNi}_3\text{@SiO}_2\text{@TiO}_2$ has high reusability and thus their application will be affordable as a catalyst in photo-catalytic processes.

4. Conclusions

The analysis of FTIR confirmed the formation of bonds in the nanocomposite. According to the analysis of XRD, the mean crystallite size of $\text{FeNi}_3/\text{SiO}_2/\text{TiO}_2$ nanocomposite was 77 nm and the FE-SEM analysis showed their tendency to agglomeration. The analysis of VSM indicated that the synthesized nanomaterial had magnetic properties. In addition, the TGA technique showed that $\text{FeNi}_3\text{@SiO}_2\text{@TiO}_2$ nanoparticles had a high resistance to heat. The results of TC degradation showed that the $\text{UV}/\text{H}_2\text{O}_2/\text{FeNi}_3/\text{SiO}_2/\text{TiO}_2$ process eliminated 100% of TC when operating at $\text{pH} = 5$, $\text{FeNi}_3/\text{SiO}_2/\text{TiO}_2$ dose = 0.01 g/L, initial TC concentration = 20 mg/L, H_2O_2 concentration = 150 mg/L, and reaction time = 90 min. Moreover, the kinetics study highlighted that the experimental data of TC degradation in the applied treatment system could be modeled by the simplified form of the Langmuir–Hinshelwood equation (pseudo-first model). As a result, the $\text{UV}/\text{H}_2\text{O}_2/\text{FeNi}_3/\text{SiO}_2/\text{TiO}_2$ process can be applied to decompose TC antibiotics appropriately in optimal conditions.

Acknowledgment

The authors of this paper acknowledge than Birjand University of Medical Sciences for their never-ending support.

References

- [1] V. Homem, L. Santos, Degradation and removal methods of antibiotics from aqueous matrices—a review, *J. Environ. Manage.*, 92 (2011) 2304–2347.
- [2] S. Bajpai, N. Chand, M. Mahendra, The adsorptive removal of a cationic drug from aqueous solution using poly(methacrylic acid) hydrogels, *Water SA*, 40 (2014) 49–56.
- [3] M. Magureanu, D. Piroi, N. Mandache, V. David, A. Medvedovici, C. Bradu, V. Parvulescu, Degradation of antibiotics in water by non-thermal plasma treatment, *Water Res.*, 4 (2011) 3407–3416.
- [4] C. Gagnon, A. Lajeunesse, P. Cejka, F. Gagne, R. Hausler, Degradation of selected acidic and neutral pharmaceutical products in a primary-treated wastewater by disinfection processes, *Ozone Sci. Eng.*, 30 (2008) 387–392.
- [5] N. Olama, M. Dehghani, M. Malakootian, The removal of amoxicillin from aquatic solutions using the TiO₂/UV-C nanophotocatalytic method doped with trivalent iron, *Appl. Water Sci.*, 8 (2018) 97.
- [6] K. Kümmerer, Antibiotics in the aquatic environment—a review—part I, *Chemosphere*, 75 (2009) 417–434.
- [7] T.J. Al-Musawi, F. Brouers, M. Zarrabi, Kinetic modeling of antibiotic adsorption onto different nanomaterials using the Brouers–Sotolongo fractal equation, *Environ. Sci. Pollut. Res. Int.*, 24 (2017) 4048–4057.
- [8] E.Y. Klein, T.P. Van Boeckel, E.M. Martinez, S. Pant, S. Gandra, S.A. Levin, H. Goossens, R. Laxminarayan, Global increase and geographic convergence in antibiotic consumption between 2000 and 2015, *Proc. Natl. Acad. Sci. U.S.A.*, 115 (2018) E3463–E3470.
- [9] M. Dehghani, S. Nasser, M. Ahmadi, M.R. Samaei, A. Anushiravani, Removal of penicillin G from aqueous phase by Fe³⁺-TiO₂/UV-A process, *J. Environ. Health Sci. Eng.*, 12 (2014) 56.
- [10] S. Chavoshan, M. Khodadadi, N. Nasseh, A.H. Panahi, A. Hosseinejad, Investigating the efficiency of single-walled and multi-walled carbon nanotubes in removal of penicillin G from aqueous solutions, *Environ. Health Eng. Manage.*, 5 (2018) 187–196.
- [11] T.P. Van Boeckel, S. Gandra, A. Ashok, Q. Caudron, B.T. Grenfell, S.A. Levin, R. Laxminarayan, Global antibiotic consumption 2000 to 2010: an analysis of national pharmaceutical sales data, *Lancet Infect. Dis.*, 14 (2014) 742–750.
- [12] J. Zhang, D. Fu, Y. Xu, C. Liu, Optimization of parameters on photocatalytic degradation of chloramphenicol using TiO₂ as photocatalyst by response surface methodology, *J. Environ. Sci.*, 22 (2010) 1281–1289.
- [13] A. Kurt, B.K. Mert, N. Özengin, Ö. Sivrioğlu, T. Yonar, Treatment of Antibiotics in Wastewater using Advanced Oxidation Processes (AOPs), *Physico-Chemical Wastewater Treatment and Resource Recovery*, IntechOpen, 2017. Available at: <https://www.intechopen.com/books/physico-chemical-wastewater-treatment-and-resource-recovery/treatment-of-antibiotics-in-wastewater-using-advanced-oxidation-processes-aops>
- [14] I. Arslan-Alaton, S. Dogruel, Pre-treatment of penicillin formulation effluent by advanced oxidation processes, *J. Hazard. Mater.*, 112 (2004) 105–113.
- [15] S. Esplugas, D.M. Bila, L.G.T. Krause, M. Dezotti, Ozonation and advanced oxidation technologies to remove endocrine disrupting chemicals (EDCs) and pharmaceuticals and personal care products (PPCPs) in water effluents, *J. Hazard. Mater.*, 149 (2007) 631–642.
- [16] J. Rivera-Utrilla, G. Prados-Joya, M. Sánchez-Polo, M. Ferro-García, I. Bautista-Toledo, Removal of nitroimidazole antibiotics from aqueous solution by adsorption/bioadsorption on activated carbon, *J. Hazard. Mater.*, 170 (2009) 298–305.
- [17] S. Norzaee, M. Taghavi, B. Djahed, F.K. Mostafapour, Degradation of penicillin G by heat activated persulfate in aqueous solution, *J. Environ. Manage.*, 215 (2018) 316–323.
- [18] M.M. McConnell, L.T. Hansen, R.C. Jamieson, K.D. Neudorf, C.K. Yost, A. Tong, Removal of antibiotic resistance genes in two tertiary level municipal wastewater treatment plants, *Sci. Total Environ.*, 643 (2018) 292–300.
- [19] J. Jeong, W. Song, W.J. Cooper, J. Jung, J. Greaves, Degradation of tetracycline antibiotics: mechanisms and kinetic studies for advanced oxidation/reduction processes, *Chemosphere*, 78 (2010) 533–540.
- [20] Y. Ji, Y. Shi, W. Dong, X. Wen, M. Jiang, J. Lu, Thermo-activated persulfate oxidation system for tetracycline antibiotics degradation in aqueous solution, *Int. J. Chem. Eng.*, 298 (2016) 225–233.
- [21] X. Wang, J. Jia, Y. Wang, Combination of photocatalysis with hydrodynamic cavitation for degradation of tetracycline, *Int. J. Chem. Eng.*, 315 (2017) 274–282.
- [22] A. Nezamzadeh-Ejhieh, A. Shirzadi, Enhancement of the photocatalytic activity of ferrous oxide by doping onto the nano-clinoptilolite particles towards photodegradation of tetracycline, *Chemosphere*, 107 (2014) 136–144.
- [23] L.S. Porubcan, C.J. Serna, J.L. White, S.L. Hem, Mechanism of adsorption of clindamycin and tetracycline by montmorillonite, *J. Pharm. Sci.*, 67 (1978) 1081–1087.
- [24] N. Oturan, J. Wu, H. Zhang, V.K. Sharma, M.A. Oturan, Electrocatalytic destruction of the antibiotic tetracycline in aqueous medium by electrochemical advanced oxidation processes: effect of electrode materials, *Appl. Catal., B*, 140 (2013) 92–97.
- [25] P. Liu, H. Zhang, Y. Feng, F. Yang, J. Zhang, Removal of trace antibiotics from wastewater: a systematic study of nanofiltration combined with ozone-based advanced oxidation processes, *Int. J. Chem. Eng.*, 240 (2014) 211–220.
- [26] E.J. Rosenfeldt, K.G. Linden, Degradation of endocrine disrupting chemicals bisphenol A, ethinyl estradiol, and estradiol during UV photolysis and advanced oxidation processes, *Environ. Sci. Technol.*, 38 (2004) 5476–5483.
- [27] W. Song, W.J. Cooper, S.P. Mezyk, J. Greaves, B.M. Peake, Free radical destruction of β -blockers in aqueous solution, *Environ. Sci. Technol.*, 42 (2008) 1256–1261.
- [28] I. Kim, H. Tanaka, Photodegradation characteristics of PPCPs in water with UV treatment, *Environ. Int.*, 35 (2009) 793–802.
- [29] I. Kim, N. Yamashita, H. Tanaka, Photodegradation of pharmaceuticals and personal care products during UV and UV/H₂O₂ treatments, *Chemosphere*, 77 (2009) 518–525.
- [30] Z. Zhu, Z. Lu, D. Wang, X. Tang, Y. Yan, W. Shi, Y. Wang, N. Gao, X. Yao, H. Dong, Construction of high-dispersed Ag/Fe₃O₄/g-C₃N₄ photocatalyst by selective photo-deposition and improved photocatalytic activity, *Appl. Catal., B*, 182 (2016) 115–122.
- [31] E. Bazrafshan, T.J. Al-Musawi, M.F. Silva, A.H. Panahi, M. Havangi, F.K. Mostafapour, Photocatalytic degradation of catechol using ZnO nanoparticles as catalyst: optimizing the experimental parameters using the Box–Behnken statistical methodology and kinetic studies, *Microchem. J.*, 147 (2019) 643–653.
- [32] M.R. Hoffmann, S.T. Martin, W. Choi, D.W. Bahnemann, Environmental applications of semiconductor photocatalysis, *Chem. Rev.*, 95 (1995) 69–96.
- [33] Y. Nosaka, T. Daimon, A.Y. Nosaka, Y. Murakami, Singlet oxygen formation in photocatalytic TiO₂ aqueous suspension, *Phys. Chem. Chem. Phys.*, 6 (2004) 2917–2918.
- [34] Y. Nosaka, S. Komori, K. Yawata, T. Hirakawa, A.Y. Nosaka, Photocatalytic OH radical formation in TiO₂ aqueous suspension studied by several detection methods, *Phys. Chem. Chem. Phys.*, 5 (2003) 4731–4735.
- [35] A. Jańczyk, E. Krakowska, G. Stochel, W. Macyk, Singlet oxygen photogeneration at surface modified titanium dioxide, *J. Am. Chem. Soc.*, 128 (2006) 15574–15575.
- [36] K. Nakata, A. Fujishima, TiO₂ photocatalysis: design and applications, *J. Photochem. Photobiol., C*, 13 (2012) 169–189.
- [37] G. Jiang, Z. Lin, C. Chen, L. Zhu, Q. Chang, N. Wang, W. Wei, H. Tang, TiO₂ nanoparticles assembled on graphene oxide nanosheets with high photocatalytic activity for removal of pollutants, *Carbon*, 49 (2011) 2693–2701.
- [38] A. Mirzaei, L. Yerushalmi, Z. Chen, F. Haghghat, Photocatalytic degradation of sulfamethoxazole by hierarchical magnetic ZnO@g-C₃N₄: RSM optimization, kinetic study, reaction pathway and toxicity evaluation, *J. Hazard. Mater.*, 359 (2018) 516–526.

- [39] E. Korina, O. Stoilova, N. Manolova, I. Rashkov, Polymer fibers with magnetic core decorated with titanium dioxide prospective for photocatalytic water treatment, *J. Environ. Chem. Eng.*, 6 (2018) 2075–2084.
- [40] M. Khodadadi, M. Ehrampoush, M. Ghaneian, A. Allahresani, A. Mahvi, Synthesis and characterizations of $\text{FeNi}_3@ \text{SiO}_2@ \text{TiO}_2$ nanocomposite and its application in photo-catalytic degradation of tetracycline in simulated wastewater, *J. Mol. Liq.*, 255 (2018) 224–232.
- [41] M. Khodadadi, M. Ehrampoush, A. Allahresani, M. Ghanian, M. Lotfi, A. Mahvi, $\text{FeNi}_3@ \text{SiO}_2$ magnetic nanocomposite as a highly efficient Fenton-like catalyst for humic acid adsorption and degradation in neutral environments, *Desal. Water Treat.*, 118 (2018) 258–267.
- [42] J. Tan, X. Wang, W. Hou, X. Zhang, L. Liu, J. Ye, D. Wang, Fabrication of $\text{Fe}_3\text{O}_4@ \text{graphene}/\text{TiO}_2$ nanohybrid with enhanced photocatalytic activity for isopropanol degradation, *J. Alloys Compd.*, 792 (2019) 918–927.
- [43] S. Xuan, W. Jiang, X. Gong, Y. Hu, Z. Chen, Magnetically separable $\text{Fe}_3\text{O}_4/\text{TiO}_2$ hollow spheres: fabrication and photocatalytic activity, *J. Phys. Chem. C*, 113 (2008) 553–558.
- [44] N. Nasseh, L. Taghavi, B. Barikbin, M.A. Nasser, Synthesis and characterizations of a novel $\text{FeNi}_3/\text{SiO}_2/\text{CuS}$ magnetic nanocomposite for photocatalytic degradation of tetracycline in simulated wastewater, *J. Cleaner Prod.*, 179 (2018) 42–54.
- [45] F. Brouers, T.J. Al-Musawi, Brouers–Sotolongo fractal kinetics versus fractional derivative kinetics: a new strategy to analyze the pollutants sorption kinetics in porous materials, *J. Hazard. Mater.*, 350 (2018) 162–168.
- [46] X. Xu, F. Ji, Z. Fan, L. He, Degradation of glyphosate in soil photocatalyzed by $\text{Fe}_3\text{O}_4/\text{SiO}_2/\text{TiO}_2$ under solar light, *Int. J. Environ. Res. Public Health*, 8 (2011) 1258–1270.
- [47] C. Yu, D. Cai, K. Yang, C.Y. Jimmy, Y. Zhou, C. Fan, Sol-gel derived S, I-codoped mesoporous TiO_2 photocatalyst with high visible-light photocatalytic activity, *J. Phys. Chem. Solids*, 71 (2010) 1337–1343.
- [48] R. Wang, X. Wang, X. Xi, R. Hu, G. Jiang, Preparation and photocatalytic activity of magnetic $\text{Fe}_3\text{O}_4/\text{SiO}_2/\text{TiO}_2$ composites, *Adv. Mater. Sci. Eng.*, 2012 (2012) 1–8, doi: 10.1155/2012/409379.
- [49] H. Khojasteh, M. Salavati-Niasari, M.-P. Mazhari, M. Hamedanian, Preparation and characterization of $\text{Fe}_3\text{O}_4@ \text{SiO}_2@ \text{TiO}_2@ \text{Pd}$ and $\text{Fe}_3\text{O}_4@ \text{SiO}_2@ \text{TiO}_2@ \text{Pd}-\text{Ag}$ nanocomposites and their utilization in enhanced degradation systems and rapid magnetic separation, *RSC Adv.*, 6 (2016) 78043–78052.
- [50] T.J. Al-Musawi, H. Kamani, E. Bazrafshan, A.H. Panahi, M.F. Silva, G. Abi, Optimization the effects of physicochemical parameters on the degradation of cephalexin in sono-Fenton reactor by using Box–Behnken response surface methodology, *Catal. Lett.*, 149 (2019) 1186–1196.
- [51] A.D. Shiraz, A. Takdastan, S.M. Borghei, Photo-Fenton like degradation of catechol using persulfate activated by UV and ferrous ions: influencing operational parameters and feasibility studies, *J. Mol. Liq.*, 249 (2018) 463–469.
- [52] P.R. Shukla, S. Wang, H.M. Ang, M.O. Tadé, Photocatalytic oxidation of phenolic compounds using zinc oxide and sulphate radicals under artificial solar light, *Sep. Purif. Technol.*, 70 (2010) 338–344.
- [53] G. Safari, M. Hoseini, M. Seyedsalehi, H. Kamani, J. Jaafari, A. Mahvi, Photocatalytic degradation of tetracycline using nanosized titanium dioxide in aqueous solution, *Int. J. Environ. Sci. Technol.*, 12 (2015) 603–616.
- [54] F. Saadati, N. Keramati, M.M. Ghazi, Influence of parameters on the photocatalytic degradation of tetracycline in wastewater: a review, *Crit. Rev. Environ. Sci. Technol.*, 46 (2016) 757–782.
- [55] M. Ahmadi, H.R. Motlagh, N. Jaafarzadeh, A. Mostoufi, R. Saeedi, G. Barzegar, S. Jorfi, Enhanced photocatalytic degradation of tetracycline and real pharmaceutical wastewater using MWCNT/ TiO_2 nano-composite, *J. Environ. Manage.*, 186 (2017) 55–63.
- [56] H.U. Rasheed, X. Lv, S. Zhang, W. Wei, J. Xie, Ternary MIL-100 (Fe)@ $\text{Fe}_3\text{O}_4/\text{CA}$ magnetic nanophotocatalysts (MNPCs): magnetically separable and Fenton-like degradation of tetracycline hydrochloride, *Adv. Powder Technol.*, 29 (2018) 3305–3314.
- [57] S. Ahmed, M. Rasul, R. Brown, M. Hashib, Influence of parameters on the heterogeneous photocatalytic degradation of pesticides and phenolic contaminants in wastewater: a short review, *J. Environ. Manage.*, 92 (2011) 311–330.
- [58] E.S. Elmolla, M. Chaudhuri, Photocatalytic degradation of amoxicillin, ampicillin and cloxacillin antibiotics in aqueous solution using UV/ TiO_2 and UV/ $\text{H}_2\text{O}_2/\text{TiO}_2$ photocatalysis, *Desalination*, 252 (2010) 46–52.
- [59] U.I. Gaya, A.H. Abdullah, Z. Zainal, M.Z. Hussein, Photocatalytic treatment of 4-chlorophenol in aqueous ZnO suspensions: intermediates, influence of dosage and inorganic anions, *J. Hazard. Mater.*, 168 (2009) 57–63.
- [60] I.R. Bautitz, R.F.P. Nogueira, Degradation of tetracycline by photo-Fenton process—solar irradiation and matrix effects, *J. Photochem. Photobiol., A*, 187 (2007) 33–39.